journal of the mechanical behavior of biomedical materials 139 (2023) 105668

Contents lists available at ScienceDirect

Journal of the Mechanical Behavior of Biomedical Materials

journal homepage: www.elsevier.com/locate/jmbbm

# Assessment of the structures contribution (crystalline and mesophases) and mechanical properties of polycaprolactone/pluronic blends

A. Tenorio-Alfonso [a], E. Vázquez Ramos [a], I. Martínez [a,*], M. Ambrosi [b], M. Raudino [b]

[a] Pro²TecS-Chemical Product and Process Technology Research Centre, University of Huelva, 21071, Huelva, Spain
[b] Department of Chemistry and CSGI, University of Florence, Via della Lastruccia 3-13, 50019, Sesto Fiorentino, Florence, Italy

ARTICLE INFO

*Keywords:*
Polycaprolactone
Pluronic
Mesophase content
Polymer blends
DSC Deconvolution
X-Ray characterization

ABSTRACT

Films of biodegradable blends of polycaprolactone (PCL) and Pluronics F68 and F127 were manufactured by an industrial thermo-mechanical process to be applied as potential delivery systems. The effects of Pluronics on the structure (mesophase organization), and thermal and mechanical properties of polycaprolactone were investigated using differential scanning calorimetry (DSC), small-angle X-ray scattering (SAXS), X-ray diffraction (XRD), polarized optical microscopy (POM) and tensile mechanical tests. The addition of Pluronics affected the crystallization process by changing the relative amounts of crystalline, amorphous, and meso- (condis + plastic) phases. The melting transition and XRD profiles were deconvoluted to assess the individual contribution of the different crystal morphologies. Furthermore, it was found that the mechanical properties of the blends depended on the ratio and type of Pluronic. Thus, Pluronic F127 showed a larger mesophase content than its F68 counterpart with PCL and blends with enhanced ductility.

## 1. Introduction

The tremendous potential of biodegradable polymers has been evinced in a wide range of exciting medical applications (drug delivery, tissue engineering, gene therapy, regenerative medicine, temporary implantable devices, and coatings on implants), so these materials are required to meet some basic criteria to be implemented as degradable biomaterials, including mechanical properties, a degradation rate appropriate for their application, non-toxic degradation products, biocompatibility, along with acceptable shelf life, stability, processability and cost (Doppalapudi et al., 2014). Such polymers, either from fossil resources like polycaprolactone or from greener raw materials, including poly(lactic acid), poly(glycolic acid), or poly(hydroxy alkanoate), have been proven to be metabolized via different routes (hydroxylation, oxidation, etc.) (De Falco et al., 2021). Among these biologically metabolizable materials, polycaprolactone (PCL), a hydrophobic polyester, excels owing to its outstanding biocompatibility, lack of toxicity before and upon hydrolysis, ease of manufacture, reasonable prices, and great permeability to a wide range of chemicals (Delgado et al., 2021; Yang et al., 2020). Thanks to these features and its low biodegradation rate and suitable mechanical resistance, PCL has been widely investigated in tissue engineering (Wang et al., 2009; Mirhosseini et al., 2016) and drug delivery systems (Pohlmann et al., 2013; Mei et al., 2009).

Biodegradation of PCL may take up from several months to years being strongly affected by supramolecular crystallinity, molecular weight, morphology, and conditions of degradation (Pantani and Sorrentino, 2013; Labet and Thielemans, 2009). Hence, a plethora of strategies, such as chemical modification or blending with other materials, enable the customization of the ultimate performance of PCL, thus fulfilling the hydrophilicity and durability required for long-term implants and drug delivery systems (Gupta et al., 2021; Bujok et al., 2021). Moreover, the process simplicity and the absence of additional reagents make bulk blending an interesting approach, given the accomplishment of a comprehensive evaluation of the polymer proportions (Mirhosseini et al., 2016; Zargarian et al., 2019).

The incorporation of a series of hydrophilic oligomers and polymers has been reported to tune the PCL polymer network, including poly (lactic acid (Balali et al., 2018), poly(glycerol sebacate) (Fakhrali et al., 2021), poly(ethylene terephthalate) (Chaparro et al., 2019) or poly (ethylene glycol) and poly(L-lactide-co-ε-caprolactone-co-glycolide) (Arbade et al., 2020). To enhance the biocompatibility and stability of PCL for drug delivery applications, the addition of amphiphilic Pluronics has been successfully pursued, avoiding phase separation between

* Corresponding author.
*E-mail address:* imgarcia@uhu.es (I. Martínez).

https://doi.org/10.1016/j.jmbbm.2023.105668
Received 8 November 2022; Received in revised form 3 January 2023; Accepted 5 January 2023
Available online 6 January 2023

hydrophilic and hydrophobic polymers, the utilization of blending solvents, and the hydrophilic leakage from the mixture upon water immersion (Li et al., 2018; Jackson et al., 2000; Werle, 2008).

Pluronics, also known as poloxamers, encompass non-ionic triblock copolymers constituted of hydrophobic propylene oxide (PPO) and hydrophilic polyethylene oxide (PEO) units arranged in a $PEO_X$-$PPO_Y$-$PEO_X$ configuration (Yang et al., 2020; Mirhosseini et al., 2016; da Rocha et al., 2019; Alexandridis and Hatton, 1995). The specific conformation of such block structure confers Pluronics to their characteristic hydrophilic-lipophilic balance (HLB), thereby enabling the tunability of their final amphiphilic properties and, by extension, those corresponding to the subsequent polymer blends (Liu et al., 2014).

Owing to their low toxicity and approval by the Food and Drug Administration (FDA), PCL/Pluronic blends have been regarded as drug delivery carriers (Hassanzadeh et al., 2014). Indeed, Mei et al. (2009) incorporated Pluronic F68 into neat PCL to overcome the docetaxel-resistance human breast adenocarcinoma MCF-7, attaining docetaxel-loaded PCL/Pluronic F68 nanoparticles with a significantly higher level of cytotoxicity against MCF-7 TAX30 breast cancer cells. Ma and Song (2007) corroborated the drug delivery enhancing effect achieved through the incorporation of Pluronic F68 into PCL microspheres for the controlled release of the anticancer chemotherapy drug paclitaxel. Additionally, Lee et al. (2020) manufactured Pluronic F127-modified PCL micropatterned 3D scaffolds for muscle tissue regeneration, using the amphiphilic poloxamer as the sacrificial agent, so that, upon water immersion, a homogeneously distributed network could be attained, characterized by a unique uniaxially aligned micro-fibrillated structure, strongly dependent on the constituents' ratio and process conditions.

Even though PCL/Pluronic blends have been proven to exhibit suitable properties for biomedical applications, they have also been regarded as promising materials in the agricultural sector. Within this framework, Assalin et al. (2019) evaluated the ecotoxicity of insecticide-loaded PCL/chitosan nanoparticles prepared via double emulsion and using Pluronics F123 and F68 as surfactants, ascertaining the more appropriate encapsulation performance of Pluronic F68 and reduced ecotoxicity when compared with commercial benchmarks.

Crystalline mesophases (liquid, plastic, and condis crystals) comprise a common state of condensed matter, characterized by an intermediate behaviour between disordered amorphous and ordered crystalline matter (Wunderlich, 1999). Additionally, the presence of crystalline mesophases confers superior stability and faster dissolution properties upon the manufactured polymer blends when compared against amorphous and pure crystalline structures, respectively, thus becoming of utmost importance for drug delivery applications (Shalaev et al., 2016). In view thereof, and despite all previous investigations, to the best of our knowledge, the understanding of the Pluronic impact over the crystallization and ultimate mechanical performance of PCL remains rather limited. Furthermore, it has to be taken into account that these investigations were based on obtaining these polymer blends as delivery systems by casting techniques rather than by thermo-mechanical industrial processing techniques as in this study.

Hence, in this study, Pluronics F68 and F127 were chosen to prepare binary biodegradable PCL/Pluronic blends with different weight ratios by extrusion and further thermoforming processes. In pursuit of a thorough evaluation of the effect of blending on the morphological features, and mechanical and thermal properties, the as-prepared films were characterized before and after long-term water immersion via differential scanning calorimetry (DSC), small-angle X-ray scattering (SAXS), X-ray diffraction (XRD), polarized optical microscopy (POM) and tensile mechanical tests.

## 2. Materials and methods

### 2.1. Materials

Polycaprolactone pellets ($M_W \sim 10^5$ g/mol), under the trade name Capa™ FB100, were kindly supplied by Perstorp Holding AB (Malmö, Sweden). Powder Pluronics F68 ($M_W \sim 8400$ g/mol, HLB = 29, solubility 100 mg/mL $H_2O$ room temperature) and F127 ($M_W \sim 12600$ g/mol, HLB = 22, solubility 50 mg/mL $H_2O$ room temperature) were provided by Sigma-Aldrich Co. (St. Louis, MO, USA). All raw materials were used as received without further purification.

### 2.2. Polymer blends preparation

Binary Pluronics/PCL mixtures were prepared using a first hot-melt extrusion process, using a fully immersed co-rotating twin-screw extruder Prism EuroLab 16 (ThermoFisher Scientific, Waltham, Massachusetts, USA), fitted with 9-barrel sections and a die (*Zones 1-10*) characterized by a 16 mm diameter and a length/diameter ratio (L/D) of 40:1. Homogeneous polymer cords were obtained using a constant screw speed of 200 rpm and the extruder temperature profiles listed in Table 1.

The addition of Pluronics was conducted by using a twin-screw volumetric feeder (Coperion K-Tron, compact KC, Switzerland), and PCL was added with a simple screw volumetric feeder (Brabender Technologie GmbH & Co. KG, Germany), leading to polymer blends containing 5 and ~9 wt% Pluronics. After visual inspection of the resulting polymer cords, systems comprising content above 8.5 and 9% w/w in Pluronic F68 and F127, respectively, were discarded given their apparent lack of homogeneity, surface irregularities, and marked brittleness. Then, the extruded polymer blends were pelletized through a Haake FLP 16 granulator (ThermoFisher Scientific, Waltham, Massachusetts, USA). The target polymer films were obtained through a compression mould process of the pelletized blends, using a hydraulic lamination hot press EQ-HP-88V-220 (MTI Corporation, Richmond, California, USA) at 85 °C and 5 MPa gauge pressure for 10 min, followed by a cooling step of 15 min at room conditions.

All blends were characterized as prepared and after aging. The aim was to compare the structural and thermal properties of fresh and aged blends and to evaluate the effect of water immersion to assess the possible applications of these biodegradable films. During the aging procedure, 0.22 ± 0.03 mm thickness polymer blend films were immersed in distilled water (0.3 ± 0.1 mg solid/g $H_2O$) within hermetic containers for at least 1 year at room conditions. Upon water immersion, loss weight values were calculated as follows:

$$Weight\ Loss = \frac{W_0 - W_\infty}{W_0} \cdot 100\% \qquad \text{Equation 1}$$

where $W_0$ and $W_\infty$ correspond to the initial and final weight (after aging), respectively. Before weighing, polymer blends were oven-dried at 120 °C for 30 min.

### 2.3. Polymer blends characterization

#### 2.3.1. Differential scanning calorimetry (DSC)

Dynamic crystallization tests were performed using a Q100 Calorimeter (TA Instruments Inc., New Castle, DE, USA). According to previous investigations (Ahmed et al., 2012), 2.5–6 mg of the specimens loaded into hermetic aluminum pans were heated up to 140 °C to erase their thermal history, followed by a cooling ramp to −80 °C and a second heating step up to 120 °C. Both thermal processes were conducted under inert nitrogen flux (50 mL $min^{-1}$) at a rate of 10 °C/min. Glass transition temperatures ($T_g$) were evaluated in the first heating ramp at the midpoint of the transition. The melting temperature ($T_m$) and the associated enthalpy change ($\Delta H_m$) were taken as the maximum temperature and the area of the peak in the heat flow curves throughout the heating

**Table 1**
Extruder barrel temperature profiles (°C) as a function of Pluronic content.

| Pluronic[a] [%] | Zone 1 | Zone 2 | Zone 3 | Zone 4 | Zone 5 | Zone 6 | Zone 7 | Zone 8 | Zone 9 | Zone 10 |
|---|---|---|---|---|---|---|---|---|---|---|
| 0 | 50 | 100 | 100 | 100 | 100 | 100 | 100 | 100 | 100 | 120 |
| >0 | 120 | 120 | 100 | 100 | 100 | 100 | 100 | 100 | 100 | 100 |

[a] Temperature profiles implemented regardless of the kind of Pluronic added.

step, respectively. From these parameters and in accordance with the previous literature (Ambrosi et al., 2019; Heeley et al., 2014), the crystallinity degree ($X_c$) of the samples can be calculated as follows:

$$X_c = \frac{\Delta H_m}{\Delta H_m^0 \cdot (1-\varphi)} \cdot 100\% \quad \text{Equation 2}$$

where $\Delta H_m^0$ is the melting enthalpy of 100% crystalline PCL, which has been estimated as 139 J $g^1$ (Pitt et al., 1981; Patricio and Bártolo, 2013), and $\varphi$ is the weight percentage of Pluronic in the sample. Additionally, the crystallinity degree associated with pure Pluronic F68 and F127 was also evaluated, presuming their 100% crystalline melting enthalpy values of 268.5 and 229.1 J $g^1$ as previously stated by Shaker et al. (2020) (Shaker et al., 2020). The crystallization process of the samples was studied as well. The characteristic crystallization temperature ($T_c$) and the corresponding enthalpy of crystallization ($\Delta H_c$) were determined as the minimum temperature of the cooling ramp and the area of the exothermic peak, respectively.

### 2.3.2. Small-angle X-ray scattering (SAXS)

SAXS measurements were performed on as-prepared PCL and blend films by a HECUS S3-MICRO camera (Kratky-type) equipped with two position-sensitive detectors (OED 50m) containing 1024 channels of 54 μm in width. Cu $K_\alpha$ radiation ($\lambda$ = 1.54 Å) was provided by an ultra brilliant point microfocus X-ray source (GENIX-Fox 3D, Xenocs, Grenoble), operating at a maximum power of 50 W. The sample-to-detector distance was 281 mm. The volume between the sample and detector was kept under vacuum conditions during the measurements to minimize the scattering from the air. The Kratky camera was calibrated in the small angle region by using silver behenate (58.34 Å). SAXS curves were obtained in the scattering vector, $q$, range between 0.01 and 0.54 $Å^{-1}$, with $q = \frac{4\pi}{\lambda} sin\,\theta$ where $\theta$ is the scattering angle. Samples were analyzed at 25 °C by using a demountable 1 mm cell having the blend films as windows. All scattering curves were corrected for the empty cell contribution by considering the relative transmission factor.

The long period of interlamellar spacing ($LP$) of the sample was determined from the Lorentz-corrected plot $I(q)q^2$ versus $q$ as $LP = 2\pi/q^*$, where $q^*$ is the peak value found in the Lorentz-corrected plot corresponding to the first order of the crystalline repeat in the spherulite (Andjelić et al., 2001).

In the lamellar stack model with a sharp phase boundary, $LP$ represents the sum of the crystal thickness ($l_c$) and the amorphous layer thickness ($l_a$). The average long period, the amorphous layer thickness, and the crystal thickness can be obtained from SAXS measurements by calculating the one-dimensional correlation function $\gamma(z)$ (Strobl and Schneider, 1980). The one-dimensional correlation function was calculated by using SasView 4.1.2 software.

### 2.3.3. X-ray diffraction (XRD)

XRD measurements on the most relevant samples were carried out at room temperature by using a Bruker D8-Da Vinci diffractometer (Cu $K_\alpha$ radiation, 40 kV × 40 mA), equipped with a Bruker LinXEYE detector, scanning range 2θ = 1.5–40°, 0.03° increments of 2θ and a time per step of 192 s.

### 2.3.4. Polarized optical microscopy (POM)

Polarized optical microscopy images were acquired by means of a Leica ICC50 W optical microscope equipped with a pair of crossed polarizers, coupled with a Linkam 420 Heating-Freezing Stage by Linkam Scientific Instruments. In order to assess the final morphology of the samples and its evolution during the non-isothermal conditions used for DSC experiments, thin layers of PCL and its blends with Pluronics were placed between glass microscope slides, heated at 200 °C for 10 min to erase their thermal history and then cooled to 25 °C with a gradient of 5 °C $min^{-1}$.

### 2.3.5. Tensile properties

Standard tensile test method UNE-EN ISO 527-3 was conducted in an AG-IS Universal Testing Machine (Shimadzu Corporation, Kyoto, Japan) fitted with a 1 kN load cell. After die-cutting the processed polymer films into dumbbell shape Type 5 (0.22 ± 0.07 mm thickness) using a die-cutting machine (ATS Faar Industries Srl, Novegro-Tregarezzo, Milan, Italy), the specimens were subjected to a crosshead speed of 50 mm $min^{-1}$ at room conditions. The obtained mechanical parameters, namely Young's modulus ($E_Y$), tensile strength ($\sigma$), and ultimate strain ($\varepsilon_{max}$) drawn from the stress-strain curves are expressed as the arithmetic mean ± standard deviation of at least five replicates of each system.

## 3. Results and discussion

### 3.1. Dynamic crystallization

Table 2 collects the thermal properties of the raw materials and the polymer blends obtained from DSC measurements under dynamic crystallization conditions, viz. glass transition temperature ($T_g$), melting temperature ($T_m$), maximum ($T_c$), and onset crystallization ($T_{onset,c}$) temperatures, along with the associated melting ($\Delta H_m$) and crystallization ($\Delta H_c$) enthalpies and the crystallinity degree ($X_c$) calculated from Equation (2).

Regardless of the Pluronic type and content, a single glass transition was found for all polymer blends. Nevertheless, given the similarities between the $T_g$s of the starting materials especially in the case of Pluronic F68 (see Table 2), no further information regarding the miscibility of Pluronics within the PCL matrix can be inferred (Kalogeras and Brostow, 2009).

Pluronics F68 and F127 are characterized by a much more intense melting peak, whose energy consumption virtually doubled as compared to pure PCL. Indeed, the melting and crystallization enthalpy values attributed to PCL/Pluronic blends remained higher than pure PCL as a consequence of Pluronics presence. Besides that, the addition of Pluronics into neat PCL seems to shift the crystallization temperatures ($T_{c1}$ and $T_{onset,c1}$) and crystallinity degree (see Fig. 1) to larger values, thus promoting the overall crystallization procedure (Li et al., 2021). This is particularly evident when adding high molecular weight Pluronic (F127) and at a higher content (see Table 2). For PCL/F127 9% blend, $T_{c1}$ raised by about 3 °C as compared to pure PCL and F127. Interestingly, $T_{c1}$ values attributed to pure materials did not significantly differ from one another.

Consequently, despite the reduced $T_{onset,c1}$ values exhibited by both pure Pluronics, their addition into neat PCL increases such thermal parameters in the polymer blends (see Table 2). In previous investigations, such an effect has been correlated with the hastening of the virgin PCL crystallization process (Ahmed et al., 2012; Zaman and Beg, 2015) with a negligible influence on the Pluronic content.

As suggested in Table 2, the energies involved in the crystallization

**Table 2**
Thermal properties of neat PCL and its Pluronics blends under dynamic calorimetric conditions.

| Sample | $T_g$ | $T_m$ | $T_{c1}$ | $T_{onset,c1}$ | $T_{c2}$ | $T_{onset,c2}$ | $\Delta H_m$ | $\Delta H_{c1}$ | $\Delta H_{c2}$ | $X_c$ |
|---|---|---|---|---|---|---|---|---|---|---|
| | (°C) | | | | | | (J/g) | | | |
| *PCL* | −59.8 | 59.9 | 32.0 | 42.7 | – | – | 67.1 | 60.0 | – | 48.3 |
| *Pluronic F68* | −59.3 | 54.4 | 30.3 | 37.0 | – | – | 134.3 | 131.2 | – | 50.0 |
| *Pluronic F127* | −65.0 | 55.9 | 31.8 | 38.7 | – | – | 119.2 | 118.1 | – | 52.0 |
| *PCL/F68 5%* | −59.6 | 60.5 | 33.5 | 42.8 | −12.5 | −8.2 | 69.3 | 59.6 | 1.2 | 52.5 |
| *PCL/F68 8.5%* | −59.7 | 58.5 | 33.5 | 41.4 | −8.9 | −1.1 | 72.2 | 54.8 | 5.2 | 56.8 |
| *PCL/F127 5%* | −62.2 | 56.8 | 35.5 | 43.5 | −8.5 | −4.0 | 70.8 | 58.9 | 2.1 | 53.6 |
| *PCL/F127 9%* | −60.6 | 57.2 | 35.3 | 43.3 | −8.3 | −3.1 | 74.4 | 59.0 | 5.5 | 58.8 |

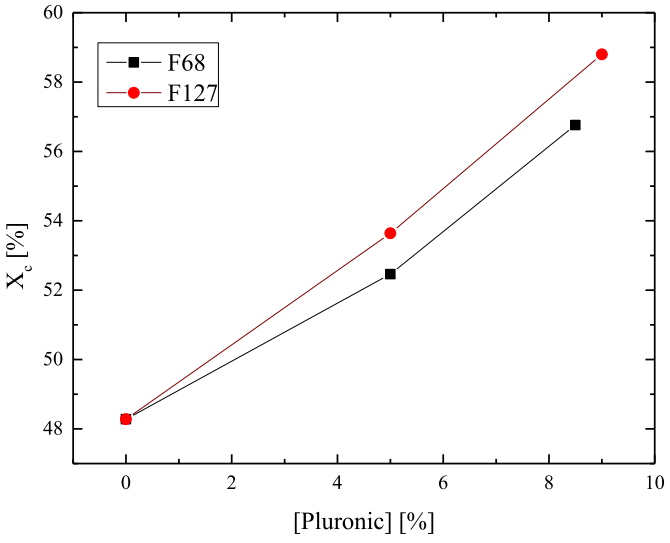


**Fig. 1.** Evolution of the crystallization degree $X_c$ with the weight percentage of Pluronic F68 and F127.

and melting processes do not correlate to each other, provided solely polymer blends are under consideration, since a second crystallization transition can be found (Fig. 2a), whose $Tc_2$s values are located in the range from −12.5 up to −8.3 °C. This thermal transition ($Tc_2$) appeared as a consequence of the introduction of Pluronic into the neat PCL, which may hinder PCL chains' movements, thus entailing a change in the crystallization process (Zhou et al., 2021). Moreover, this additional crystallization peak not only relies on the introduction of Pluronic into the neat PCL but also on the extent to which they were added. Indeed, higher Pluronic loads gave rise to fostered the second crystallization process characterized by a larger energy release ($\Delta Hc_2$) and greater characteristic temperature values ($T_{c2}$ and $T_{onset,c2}$).

Furthermore, PCL is usually described as a semicrystalline polymer containing spherulites with an orthorhombic chain packing (Chatani et al., 1970). Nevertheless, as for other biopolymers, such as poly(lactic acid), the presence of partially ordered mesophases has been proposed as the result of processing (Stoclet et al., 2010). Both plastic and condis crystal mesophases have been previously discussed for PCL (Wunderlich, 1999; Selli et al., 2020; Baptista et al., 2020). Thus, bearing that in mind and aiming at delving into the impact of adding Pluronic into neat PCL, the melting transition has been suitably deconvoluted into three Gaussian peaks to evaluate the individual contribution of the likely different crystal morphologies. Fig. 3 shows the deconvolution of the melting peak for PCL modified with a 9% of Pluronic F127 as an example. The melting temperatures and the relative percentage contributions resulting from the deconvolution process are gathered in Table 3.

As can be seen from these results, thermograms for all investigated samples – including neat PCL – could be successfully deconvoluted by

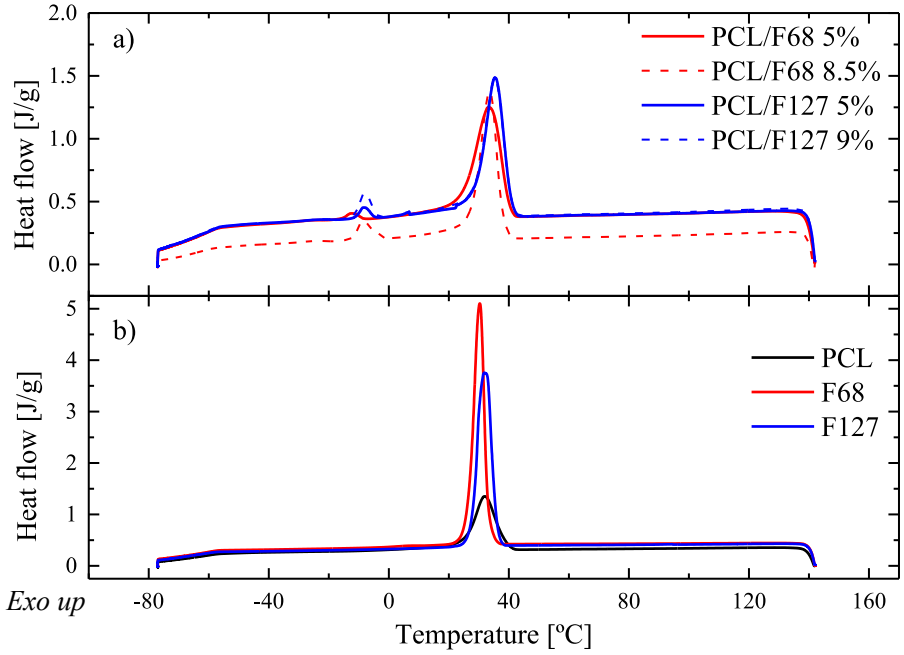


**Fig. 2.** DSC thermograms resulting from the first cooling ramp for the studied polymer blends (a) and raw materials (b).

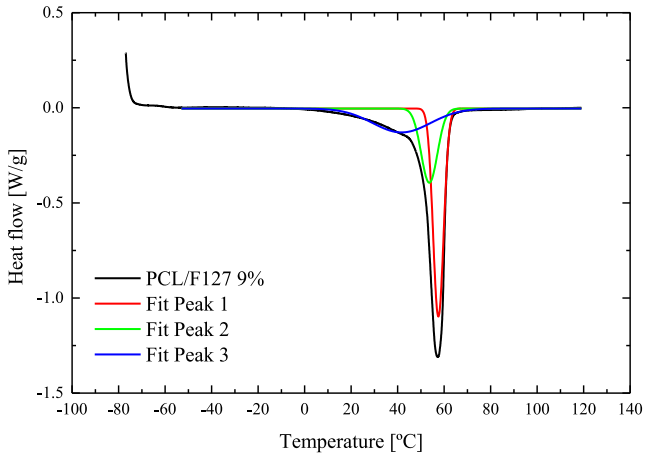


**Fig. 3.** Melting peak deconvolution for polymer blend PCL/F127 9%.

**Table 3**
Deconvolution results in terms of melting temperatures and percentages of the different contributions.

| Sample | $T_{m1}$ | $T_{m2}$ | $T_{m3}$ | $A_1$ [%] | $A_2$ [%] | $A_3$ [%] |
|---|---|---|---|---|---|---|
| *PCL* | 43 | 56 | 60 | 40.0 | 30.3 | 29.6 |
| *PCL/F68 5%* | 45 | 58 | 62 | 36.6 | 49.1 | 14.3 |
| *PCL/F68 8.5%* | 44 | 56 | 59 | 34.6 | 49.9 | 15.5 |
| *PCL/F127 5%* | 41 | 53 | 57 | 33.0 | 24.3 | 42.7 |
| *PCL/F127 9%* | 42 | 54 | 58 | 28.9 | 25.3 | 45.7 |

using three Gaussian components, indicating the presence of different crystal morphologies within the formed crystallites. The addition of Pluronics was found to affect the crystallization process changing the relative amounts of the different crystalline morphologies. In particular, the crystalline phase whose $T_m$ is located at around 56-58 °C seems to be formed preferentially (see Table 3).

Additionally, considering the high water solubility of Pluronics, along with the negligible hydrolysis of PCL in distilled water (Lu et al., 2018), the weight loss of each sample was measured after one year of immersion in distilled water (Table 4) as an indirect measurement of the Pluronics' leaching from the PCL matrix into the aqueous phase, besides its impact on the PCL/Pluronic blends crystallization.

Weight loss data showed a considerable reliance on the Pluronic nature, indeed the highest polymer mass loss was observed for samples with Pluronic F68. Besides, the weight reduction seems to increase from a Pluronic concentration higher than 5%, which may be due to the dilution of the Pluronic excess in the blend ratio. The dependence of weight loss on the type of Pluronic could be due to interactions established between the polymeric chains of PCL and Pluronic: The results may suggest stronger interactions between Pluronic F127 and PCL than for PCL and F68. Thereby different PCL crystalline morphologies may be produced, which, for PCL/F127 blend compositions, hamper the release

**Table 4**
wt loss assessed after a long-term water immersion of PCL/Pluronic polymer blends.

| *Samples* | *Initial weight (mg)* | *Wet weight (mg)* | *Weight after drying (mg)* | *Weight loss (%)* |
|---|---|---|---|---|
| *PCL/F68 5%* | 21.5 | 21.3 | 21.0 | 2.2 |
| *PCL/F68 8.5%* | 28.1 | 27.2 | 25.8 | 8.2 |
| *PCL/F127 5%* | 38.4 | 38.8 | 38.3 | 0.3 |
| *PCL/F127 9%* | 15.0 | 14.8 | 14.2 | 5.2 |

of Pluronic F127 into the aqueous medium (see Table 4). Moreover, the previously mentioned slightly larger decrease in melting temperature for blends containing Pluronic F127 seems to support this hypothesis as well.

Dynamic DSC tests on PCL/Pluronics blends after water immersion (Table 5) supported the hypothesized nucleating effect of Pluronics, as deducible by the apparent reduction in the crystallinity degree and the characteristic $T_{onset,c1}$ and $T_{onset,c2}$ parameters, due to the likely Pluronic release into the water. As can be observed, the crystallinity degree of the blends diminished after immersion in water, especially for Pluronic F127-based blends. Therefore, water immersion generally leads to reduced crystallization enthalpies ascribed to both crystallization steps ($\Delta H_{c1}$ *and* $\Delta H_{c2}$) (Table 2), suggesting that, although long-term water immersion affects both crystalline phases, that crystallization event featured by $T_{c2}$ is strictly related to the presence of Pluronic since it occurs only for PCL/Pluronic blends and is not visible for neat PCL thermograms.

F68/PCL blends would be expected to show a more significant reduction in crystallinity owing to their larger leaching into water (Table 4). Nevertheless, this reduction is more noticeable in F127-bearing samples. As a consequence of the synergetic effect of the high water solubility and the more important additive-neat PCL interactions, long-term water immersion of the latter may involve some water entrapment within the polymer matrix, hence increasing their amorphous phase, as confirmed later on by XRD results (see section 3.2.2). Thus, it could be hypothesized that the water effect resides in partial or full solubilization of Pluronic-crystalline domains.

In an effort to draw relationships between the microstructure of the blends and their behavior in water, the melting peaks after water immersion were also deconvoluted (Table 6) and henceforth discussed against previous results. The most evident change after immersion of the blends in water is the reduction of the melting peak 3 areas for PCL modified with Pluronic F68. Furthermore, these blends show the highest weight loss after immersion in water. This result may suggest that Pluronic F68 contributes to the formation of the crystal morphology corresponding to melting peak 3. Differently, in the case of F127 blends, it seems that the crystalline structure of the blends is not remarkably affected by water immersion, as evidenced by the presence of their respective typical crystalline peaks upon immersion. This observation supports the hypothesis that the higher chemical compatibility between PCL and Pluronic F127 is responsible for stronger interactions between the polymer and the amphiphile, hence reducing the leaching of Pluronic out from the PCL matrix after long contact with water if compared with the case of F68-based bends compositions.

### 3.2. X-Ray investigation

#### 3.2.1. As-prepared films

The nano and microstructure of neat PCL and its Pluronics blends were investigated through X-ray measurements. Long-range order was assessed by small angle X-ray scattering (SAXS), while the sub-cell packing was determined by X-ray diffraction (XRD).

SAXS profiles of neat PCL and the as-prepared blends are shown in SI (Fig. S1 in Online Resource), while Fig. 4 shows the Lorentz-corrected plots $I(q)q^2$ versus q. All samples showed one peak at about q = 0.04 $Å^{-1}$ due to the first order of the crystalline lamellar repeat (or long period, *LP*). A subtle shift of this peak toward larger q values is observed for all blends as compared to neat PCL. *LP* extracted from Bragg law was 16.5 nm for neat PCL and about 15.5 nm for all blend compositions.

The obtained *LP* values are reported in Table 7 together with the morphological parameters, namely long period (*L*), the thickness of the crystalline layer ($l_c$), and the thickness of the amorphous layer ($l_a$), associated with the lamellar domains obtained from the calculation of the 1D-correlation function ($\gamma(z)$).

The addition of Pluronics led to a subtle decrease of the overall lamellar thickness (~1−2 nm) accompanied by a shrinkage of the

**Table 5**
Thermal properties of the evaluated polymer blends under dynamic calorimetric conditions after water immersion.

| Sample | $T_m$ | $T_{c1}$ | $T_{onset,c1}$ | $T_{c2}$ | $T_{onset,c2}$ | $\Delta H_m$ | $\Delta H_{c1}$ | $\Delta H_{c2}$ | $X_c$ |
|---|---|---|---|---|---|---|---|---|---|
| | (°C) | | | | | (J/g) | | | |
| *PCL/F68 5%* | 56.0 | 34.8 | 37.8 | −20.3 | −12.8 | 65.7 | 58.57 | 1.6 | 49.8 |
| *PCL/F68 8.5%* | 55.8 | 34.4 | 36.9 | −20.8 | −14.0 | 63.9 | 58.16 | 1.0 | 50.3 |
| *PCL/F127 5%* | 56.0 | 34.8 | 38.1 | −10.4 | −6.9 | 59.2 | 54.2 | 0.4 | 44.8 |
| *PCL/F127 9%* | 55.9 | 34.7 | 37.6 | −17.7 | −6.3 | 57.5 | 51.5 | 1.9 | 45.5 |

**Table 6**
Deconvolution results after water immersion in terms of melting temperatures ($T_{mi}$) and percentages of the different contributions ($A_i$).

| Sample | $T_{m1}$ | $T_{m2}$ | $T_{m3}$ | $A_1$ [%] | $A_2$ [%] | $A_3$ [%] |
|---|---|---|---|---|---|---|
| *PCL/F68 5%* | 46 | 57 | 62 | 41.7 | 58.3 | 0.0 |
| *PCL/F68 8.5%* | 46 | 56 | 59 | 48.2 | 46.5 | 5.3 |
| *PCL/F127 5%* | 41 | 53 | 57 | 33.0 | 24.3 | 42.7 |
| *PCL/F127 9%* | 42 | 53 | 57 | 39.0 | 19.7 | 41.3 |

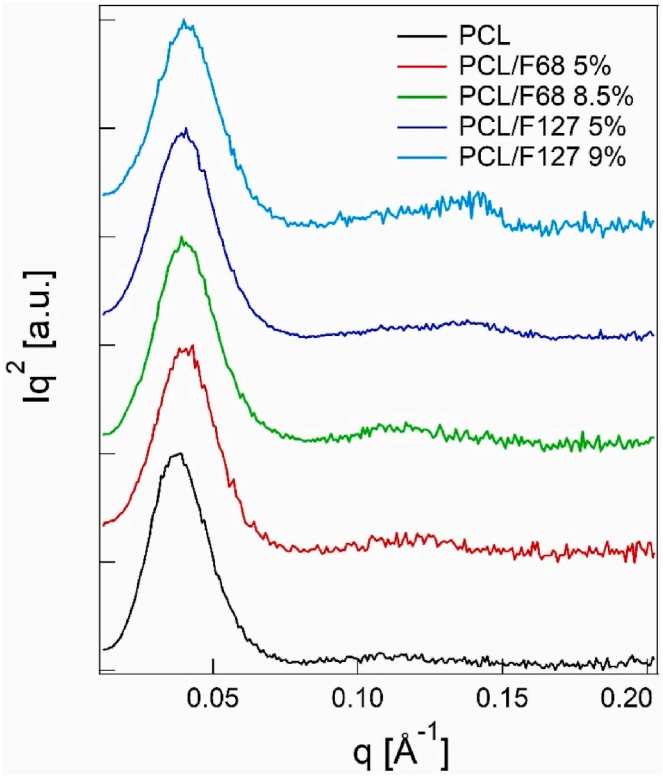


**Fig. 4.** Lorentz-corrected plots for neat PCL and PCL/Pluronic blend compositions. The curves have been displaced along the y-axis for clarity.

**Table 7**
Structural parameters for neat PCL and PCL/Pluronics blends: long period, LP, obtained from Lorentz-corrected plots, long period, L, the thickness of crystalline and amorphous layers ($l_c$ and $l_a$, respectively) obtained from 1D-correlation function.

| Sample | *LP* (nm) | *L* (nm) | $l_c$ (nm) | $l_a$ (nm) |
|---|---|---|---|---|
| PCL | 16.5 | 15.7 | 7.7 | 8.0 |
| PCL/F68 5% | 15.4 | 13.1 | 5.1 | 8.0 |
| PCL/F68 8.5% | 15.4 | 13.6 | 4.6 | 9.0 |
| PCL/F127 5% | 15.4 | 14.5 | 5.3 | 9.2 |
| PCL/F127 9% | 15.7 | 13.6 | 4.8 | 8.8 |

crystalline layer, whose dimension changed from 7.7 nm for neat PCL to about 5 nm in the blends. The amorphous layer, instead, was found to remain approximately constant or slightly increased for blend compositions. This finding may suggest a variation of PCL crystallization behavior imparted by Pluronics featured by a decrease of sample crystallinity ascribable to the lamellar arrangement.

SAXS analysis also provides an estimation of the crystallinity associated with lamellar domains, the so-called linear crystallinity ($\varphi_c^{lin}$), which can be determined as $l_c/L$ (Chen and Hsiao, 1998). The values of $\varphi_c^{lin}$ for neat PCL and all blend compositions are reported in Table 8, together with the crystallinity determined by DSC ($X_{c,DSC}$) and XRD ($X_{c,XRD}$) measurements.

It can be noted that there is a good agreement between the crystallinity values obtained from the different techniques for neat PCL. This result suggests that, for the homopolymer, the crystallinity mostly resides within the lamellar domains. Indeed, SAXS only probes the crystallinity inside lamellar stacks, while DSC and XRD account for the overall sample crystallinity. To further corroborate this hypothesis, we calculated the volume fraction of lamellar stacks in the sample ($\varphi_s$), that, for volume-filling spherulites, can be obtained by comparing the linear crystallinity from SAXS ($\varphi_c^{lin}$) to the bulk crystallinity ($\varphi_c$) according to Equation (3) (Zhu et al., 2004):

$$\varphi_c = \varphi_s \bullet \varphi_c^{lin} \qquad \text{Equation 3}$$

where $\varphi_c$ is calculated from the crystallinity degree obtained by DSC, $X_{c,DSC}$, as follows (Kurusu et al., 2014):

$$\varphi_c = X_{c,DSC}\left(\frac{\rho_s}{\rho_c}\right) \qquad \text{Equation 4}$$

corresponding $\rho_s$ and $\rho_c$ to the overall and crystalline fraction densities, respectively. Additionally, the overall density $\rho_s$ can be calculated by the following equation:

$$\rho_s = X_c\rho_c + (1 - X_c)\rho_a \qquad \text{Equation 5}$$

where $\rho_a$ is the density of the amorphous phase. The calculation can be solved only for pure PCL since $\rho_c$ and $\rho_a$ values are not available for Pluronics F68 and F127. The values used for $\rho_c$ and $\rho_a$ for neat PCL are 1.195 and 1.081 g cm$^{-3}$, respectively (Ketelaars et al., 1997).

The calculated values of $\varphi_c$ and $\varphi_c^{lin}$ for neat PCL were 0.459 and 0.483, respectively, which led to $\varphi_s = 0.95$, only slightly lower than unity. This $\varphi_s$ value indicates that, for neat PCL, the volume is substantially homogeneously filled with lamellar stacks and only a small portion of crystallinity resides in different morphologies (Zhu et al., 2004).

For PCL/Pluronics blends, the crystallinity values from DSC and XRD agreed well, while the crystallinity determined from SAXS 1D-correlation function was significantly lower. This is certainly due to the shrinkage of the crystalline layer $l_c$ upon Pluronics addition, but it could also indicate the existence of crystals not arranged as lamellar layers. Indeed, SAXS accounts only for the crystallinity inside lamellar stacks, and, poorly crystallized domains with ill-defined lamellar structures or differently arranged crystals might contribute to the overall crystallinity detected by DSC and XRD, but they might be invisible to SAXS, thus explaining the observed discrepancies in the overall crystallinity of the

**Table 8**
Linear crystallinity ($\varphi_c^{lin}$), crystallinity degree obtained by DSC($X_{c,DSC}$), crystallinity degree obtained by XRD ($X_{c,XRD}$), and phase contents as determined by fitting of XRD profiles.

| Sample | $\varphi_c^{lin}$ | $X_{c,DSC}$ | $X_{c,XRD}$ | | | |
|---|---|---|---|---|---|---|
| | | | Amorphous (%) | Crystalline (%) | Lamellar cryst. (%) | Mesophases (%) |
| PCL | 48.9 | 48.3 | 47.8 | 52.2 | 47.4 | 4.8 |
| PCL/F68 5% | 38.6 | 52.5 | 58.2 | 41.8 | 32.4 | 9.4 |
| PCL/F68 8.5% | 33.8 | 56.8 | 46.7 | 53.3 | 44.9 | 8.4 |
| PCL/F127 5% | 36.5 | 53.6 | 46.8 | 53.2 | 40.3 | 12.9 |
| PCL/F127 9% | 35.1 | 58.8 | 43.8 | 56.2 | 41.5 | 14.7 |

blends obtained by different techniques.

XRD was performed on the same films investigated by SAXS to obtain a qualitative and quantitative description of their morphology at the microscale. Recently, Baptista et al. reported the formation of mesophases by the application of pressure at various temperatures and periods on PCL (Baptista et al., 2020). In particular, the authors argued that four different morphologies occur depending on the processing parameters: crystalline, condis crystal mesophase, plastic crystal mesophase, and amorphous. A quantitative analysis of the XRD profiles enabled the determination of the content of crystalline, amorphous, and mesophase (condis + plastic) phases. Our experimental XRD profiles obtained on as-prepared PCL and blend films are reported in Fig. 5.

All samples show an orthorhombic structure as indicated by the two characteristic peaks at 2θ values of 21° and 24.5° that dominate all XRD patterns. These reflections are attributed to the (110) and (200) planes, respectively. An additional small peak at 22° ascribable to the (111) plane of the orthorhombic unit cell is also visible (Vergara-Porras et al., 2016). A partial amorphous character can be inferred by the broad feature centered around 12.5°, more significant for neat PCL than for

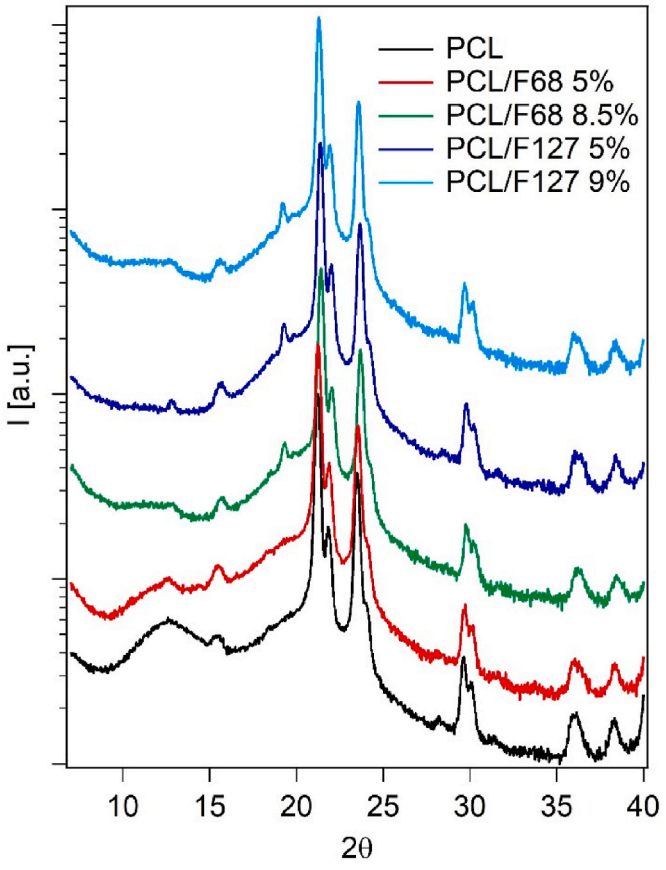


**Fig. 5.** XRD patterns for neat PCL and PCL/Pluronics blend compositions. The curves have been displaced along the y-axis for clarity.

blend compositions (Baptista et al., 2020).

All blends, except for PCL/F68 5%, also show a small peak at about 19° attributable to crystalline Pluronics (see Fig. S2 in Online Resource) (Li et al., 2018). This small peak may correlate with the small extra crystallization peak featured by $T_{c2}$ observed on blends' thermograms. It could be hypothesized that a tiny amount of Pluronic crystallizes at a lower temperature, in a somehow confined environment, being its crystallization hindered by the surrounding PCL. Besides, according to DSC investigations performed on samples immersed in water, this phase is that mainly involved leaching, at least for blends containing a higher amount of Pluronics and especially for the PCL/F68 8.5% sample.

All XRD patterns were deconvoluted to quantitatively analyze the contribution of four different phases: crystalline, mesophase (condis and plastic crystals), and amorphous, according to the method previously described in the literature (Stoclet et al., 2010) (see Fig. S3 in Online Resource). The so-obtained crystalline, amorphous, and mesophase contents are reported in Table 8, together with the crystallinity degrees obtained by both SAXS and DSC analysis. As already mentioned, the overall crystallinity determined by XRD agrees with values determined by DSC suggesting that all crystal morphologies contribute to the XRD signal and share an orthorhombic arrangement of the polymer chains. Only PCL/F68 5% slightly deviates from this trend, but it is worthwhile to note that an inconstant behavior was recorded for this sample both by SAXS and XRD. The mesophase content increases upon blending, doubling, and tripling by the addition of F68 and F127, respectively. Indeed, blending may result in an increased conformational disorder, thus hindering the chain-folding which leads to lamellar crystals. In the mesophases, polymer chains maintain the positional order adopting an orthorhombic packing but lose part of the conformational order with the formation of ill-defined lamellar folds.

PCL is known to crystallize in orthorhombic dendritic spherulites although large spherulites are hardly observed (Baptista et al., 2020). Indeed, no structural features may be seen on the micrograph of PCL alone (see Fig. 6, left). It is also well known that polymer morphology strongly depends on crystallization conditions. Morphology can change when the polymer is solidified from melt or solution, as well as morphological changes may be induced by temperature processing or through the application of stress or strain. In the present case, Pluronics, particularly F127, seems to introduce a partial degree of orientational order (typical of condis mesophase) as also corroborated by the increased birefringence observed by POM for PCL/F127 blends (see Fig. 6, right).

The formation of mesophases with poor lamellar packing contributes to explain the lost crystallinity determined by SAXS fitting and, therefore, the significantly lower crystallinity degree obtained by SAXS as compared to DSC and XRD. The crystallinity associated with lamellar domains obtained by XRD is slightly larger than that determined by SAXS but still significantly lower than the overall crystallinity, which also includes the contribution of conformationally disordered mesophases. It is worthwhile to mention that small discrepancies may be expected since the measurement technique is known to influence the obtained absolute crystallinity values (Selli et al., 2020). Despite the increase in the overall crystallinity imparted by the addition of Pluronics, plastic and condis crystals may be formed upon blending at the

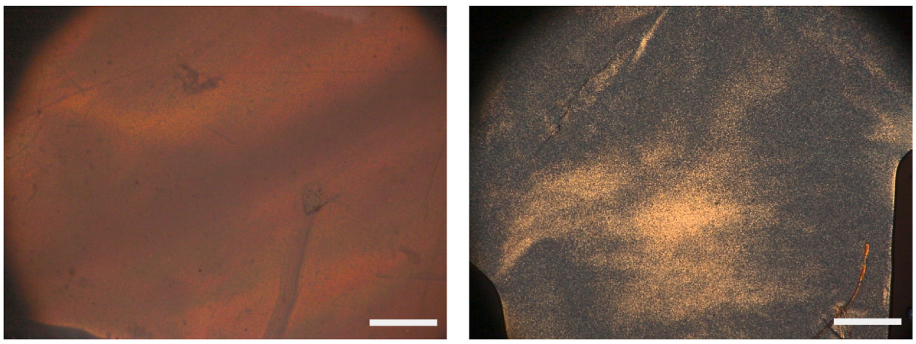

**Fig. 6.** Polarized optical microscopy images of neat PCL (left) and PCL/F127 9% blend (right) acquired at 25 °C. Magnification: 5×, scale bar = 50 μm.

expense of spherulites. F127 is less hydrophilic than F68 (HLB = 22 and 29, respectively) and possesses a larger molecular weight. The lower diffusion coefficient and its possible higher compatibility with hydrophobic PCL may hinder the F127 escape from the spherulite envelope during crystallization, thus favoring the formation of more disordered mesophases. The presence of mesophases is also confirmed by calorimetry, as inferred from Fig. 3, denoting the appearance of different melting peaks ascribed to several crystal morphologies.

### 3.2.2. *After long-term immersion in water*

XRD analysis was performed on blends after immersion in water. The recorded patterns are reported in Fig. 7.

For all blends, the width of the peaks attributed to the (110) and (200) faces of orthorhombic crystals increases as a result of an increased structural disorder. The amorphous character of blends is also increased as indicated by the broad feature at about 12°. Thus, the profiles agree with the lower crystallinity degree determined by DSC (Table 5). The most significant change is recorded for PCL/F68 8.5% blend, for which the profile of the peak around 21° assigned to the (110) planes splits into a double peak (see also Fig. S4 in Online Resource). XRD patterns recorded after water immersion were also deconvoluted through Gaussian curves to determine the mesophase content (Table S1). While the amount of plastic and condis crystals remains approximately constant for blends containing F127, the mesophase percentage strongly increases in the presence of F68, in particular, for PCL/F68 8.5% for which the mesophase content increases from about 8 to about 20% after immersion in water. Although further investigations are undergoing in order to better understand the leaching process, it is worthwhile to note that PCL/F68 8.5% blend is mostly affected by water immersion, as also shown by DSC results.

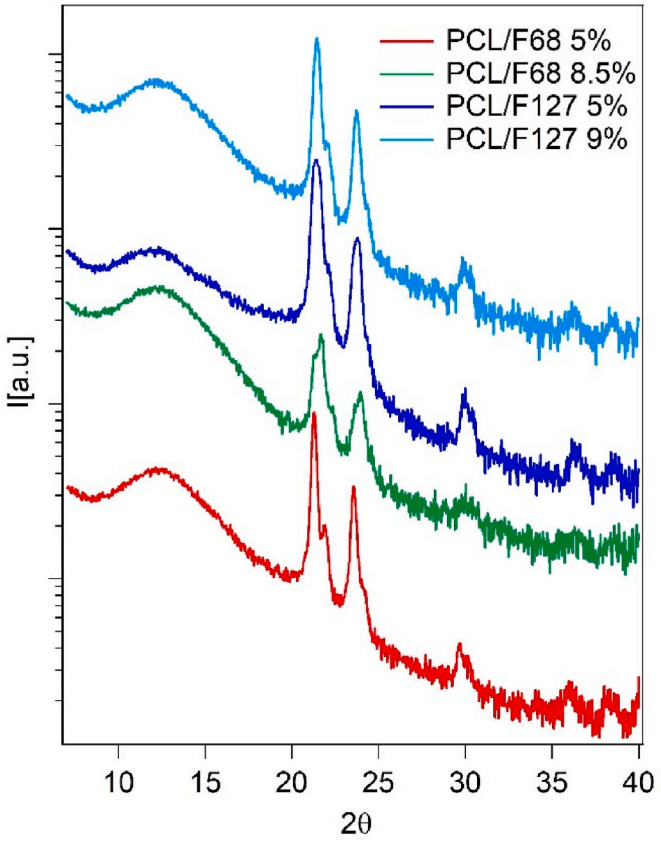


**Fig. 7.** XRD patterns for PCL/Pluronics blend compositions after water immersion. The curves have been displaced along the y-axis for clarity.

### 3.3. *Mechanical behaviour*

The mechanical response under tensile deformation of the studied biodegradable polymer blends is reported in Table 9.

The addition of Pluronic to neat PCL, regardless of its nature or amount, provides the PCL with a decreased rigidity, which is mainly detectable by the reduction of Young's modulus of the blends compared to neat PCL, in agreement with previous investigations (Rychter et al., 2019; Wu et al., 2018). However, although the blend containing 5% Pluronic F68 develops the highest Young's modulus, a marked reduction of this mechanical parameter is obtained when the F68 content is increased to 8.5%. On the other hand, PCL/F127 blends show comparable $E_Y$ values independently from F127 concentration. Although an increase in crystallinity generally raises the modulus of elasticity, we observe a reduction in the modulus of PCL/Pluronic samples even if the blends are featured by higher crystallinity degree values. A possible explanation for this unexpected behaviour can arise from the higher development of mesophases in these blends and the modification of the morphology with the formation of more disordered crystals (Selli et al., 2020).

Concerning tensile strength, PCL modified with low loads of Pluronic exhibits a slightly higher mechanical resistance compared to pure PCL, presumably due to the capability of the mesophase content to take up most of the forces and evenly distribute it between rigid crystals (Selli et al., 2020).

For PCL/F127 5% sample, the increased tensile strength may also

**Table 9**
Tensile properties of the compression molded polymer blends.

| Sample | $E_Y$ (MPa) | σ (MPa) | $\varepsilon_{Max}$ (%) |
|---|---|---|---|
| *PCL* | 315.72 ± 44.07 | 24.78 ± 4.77 | 692.56 ± 105.76 |
| *PCL/F68 5%* | 289.91 ± 60.86 | 27.69 ± 7.72 | 671.52 ± 252.67 |
| *PCL/F68 8.5%* | 252.18 ± 16.33 | 11.23 ± 1.52 | 67.44 ± 65.86 |
| *PCL/F127 5%* | 257.38 ± 31.20 | 27.19 ± 3.66 | 768.68 ± 74.02 |
| *PCL/F127 9%* | 256.19 ± 36.25 | 22.44 ± 2.22 | 698.86 ± 26.48 |

come from the enhancement of the polymer chain cohesion and adhesion due to the partial incorporation of Pluronic F127 into the PCL matrix. However, the addition of a greater Pluronic content in the polymer blend formulation yielded polymeric systems with a diminished mechanical response, which becomes remarkable for PCL/F68 8.5% blend, which exhibited a 59% reduction in the tensile strength. Sample microscopic heterogeneity may be assumed to increase when raising the Pluronic content with the formation of Pluronic-rich domains. Indeed, phase boundaries between different phases may concur in decreasing the mechanical performance, as particularly evident for PCL/F68 8.5% blend. Furthermore, the PCL/F68 8.5% blend was found to be most affected by the long-term water immersion, possibly supporting the hypothesis of the formation of pluronic-rich domains which may act as structural heterogeneities that weaken the mechanical resistance.

It should be noted that samples with high elongation at break ($\varepsilon_{Max}$), i.e., PCL/F127 blends, have the largest mesophase content. It is suspected that the mesophase contributes to the enhanced ductility of PCL/Pluronic F127 blends. The highest elongation was close to 700%, obtained for PCL/F127 5% sample. According to POM results, this system seems to introduce a partial degree of crystal orientation, an effect to be considered in the mechanical properties. On the other hand, the formation of mesophase would also indicate the important role of mesophase in determining the post-yielding behaviour of PCL/Pluronics blends (Selli et al., 2020).

As can be inferred from mechanical properties, there might be a threshold for Pluronic content, above which the blends show a drastic reduction of their mechanical behaviour (Wu et al., 2018) due to the reduction of polymer/polymer interactions caused by the diluent effect of Pluronics. In addition, we demonstrated that the presence of Pluronics modifies the types of crystals formed in PCL by favouring plastic and condis crystals that are characterized by an increased disorder, thus lowering Young's modulus and tensile strength of the blends if compared to the neat PCL.

## 4. Conclusions

In this investigation, binary polymer blends of PCL with Pluronics F68 and F127 (5-9%) were developed through an extrusion and subsequent thermoforming mechanical processing techniques, and the organizational structure and thermo-mechanical response of the ensuing films were comprehensively characterized.

The addition of both Pluronics to PCL was proven to promote crystallization, raising the blend's crystallinity degree by almost 10% at the highest Pluronics' load (9%). Moreover, although pure PCL typically crystallizes according to a lamellar arrangement, upon the incorporation of Pluronics, the increase in the proportion of disordered plastic and condis crystal mesophases to the detriment of the lamellar stacks spherulites was evinced. Therefore, the binary blends prepared by adding the lowest Pluronic amount (5%) exhibited an unexpected, reduced rigidity, along with improved tensile strength. Furthermore, the enhancement of the mesophase content was proven to favour ductility, especially when considering Pluronic F127. However, the fostered production of disordered plastic and condis mesophases obtained through the addition of both Pluronics highlighted the appearance of a Pluronic content threshold, above which a marked loss in their mechanical response was denoted.

On the other hand, the stronger compatibility of Pluronic F127 with PCL, as compared to its F68 counterpart, was supported not only by the more significant reduction in the $T_g$ of PCL/F127 polymer blends but also by their reduced weight loss after long-term water immersion, bearing in mind that water seemed to preferentially dissolve Pluronic-rich domains. Consequently, no significant impact on the deconvoluted melting peaks of PCL/F127 blends after immersion was observed, in contrast with the complete disappearance of the melting peak centered at 62 °C attributed to the system PCL/F68 5%.

## CRediT authorship contribution statement

**A. Tenorio-Alfonso:** Writing – review & editing, Writing – original draft, Visualization, Validation, Supervision, Resources, Project administration, Methodology, Investigation, Formal analysis, Data curation, Conceptualization. **E. Vázquez Ramos:** Writing – original draft, Methodology, Formal analysis, Data curation, Conceptualization. **I. Martínez:** Writing – review & editing, Writing – original draft, Visualization, Validation, Supervision, Resources, Project administration, Methodology, Investigation, Formal analysis, Data curation, Conceptualization. **M. Ambrosi:** Writing – review & editing, Writing – original draft, Visualization, Validation, Supervision, Resources, Project administration, Methodology, Investigation, Formal analysis, Data curation, Conceptualization. **M. Raudino:** Writing – review & editing, Writing – original draft, Visualization, Validation, Supervision, Resources, Project administration, Methodology, Investigation, Formal analysis, Data curation, Conceptualization.

## Declaration of competing interest

The authors declare that they have no known competing financial interests or personal relationships that could have appeared to influence the work reported in this paper.

## Data availability

Data will be made available on request.

## Acknowledgements

Funding for open access charge was provided by Universidad de Huelva/CBUA. The authors gratefully acknowledge the financial support.

## Appendix A. Supplementary data

Supplementary data to this article can be found online at https://doi.org/10.1016/j.jmbbm.2023.105668.

## References

Ahmed, J., Auras, R., Kijchavengkul, T., Varshney, S.K., 2012. Rheological, thermal and structural behavior of poly (ε-caprolactone) and nanoclay blended films. J. Food Eng. 111 (4), 580–589. https://doi.org/10.1016/j.jfoodeng.2012.03.014.

Alexandridis, P., Hatton, T.A., 1995. Poly (ethylene oxide)□ poly (propylene oxide)□ poly (ethylene oxide) block copolymer surfactants in aqueous solutions and at interfaces: thermodynamics, structure, dynamics, and modeling. Colloids Surf Physicochem Eng Aspects 96 (1-2), 1–46. https://doi.org/10.1016/0927-7757(94)03028-X.

Ambrosi, M., Raudino, M., Diañez, I., Martínez, I., 2019. Non-isothermal crystallization kinetics and morphology of poly (3-hydroxybutyrate)/pluronic blends. Eur. Polym. J. 120, 109189 https://doi.org/10.1016/j.eurpolymj.2019.08.016.

Andjelić, S., Jamiolkowski, D., Mcdivitt, J., Fischer, J., Zhou, J., Wang, Z., Hsiao, B.S., 2001. Time-resolved crystallization study of absorbable polymers by synchrotron small-angle X-ray scattering. J. Polym. Sci. B Polym. Phys. 39 (1), 153–167. https://doi.org/10.1002/1099-0488(20010101)39:13.0.CO;2-9.

Arbade, G.K., Srivastava, J., Tripathi, V., Lenka, N., Patro, T.U., 2020. Enhancement of hydrophilicity, biocompatibility and biodegradability of poly (ε-caprolactone) electrospun nanofiber scaffolds using poly (ethylene glycol) and poly (L-lactide-co-ε-caprolactone-co-glycolide) as additives for soft tissue engineering. J. Biomater. Sci. Polym. Ed. 31 (13), 1648–1670. https://doi.org/10.1080/09205063.2020.1769799.

Assalin, M.R., dos Santos, L., Souza, D., Rosa, M.A., Duarte, R., Castanha, R.F., Donaire, P., Durán, N., 2019. Ecotoxicity evaluation: preparation of poly-ε-caprolactone and chitosan nanoparticles as carriers of thiamethoxam. pesticide 1323 (1), 012017.

Balali, S., Davachi, S.M., Sahraeian, R., Shiroud Heidari, B., Seyfi, J., Hejazi, I., 2018. Preparation and characterization of composite blends based on polylactic acid/polycaprolactone and silk. Biomacromolecules 19 (11), 4358–4369. https://doi.org/10.1021/acs.biomac.8b01254.

Baptista, C., Azagury, A., Shin, H., Baker, C.M., Ly, E., Lee, R., Mathiowitz, E., 2020. The effect of temperature and pressure on polycaprolactone morphology. Polymer 191, 122227. https://doi.org/10.1016/j.polymer.2020.122227.

Bujok, S., Peter, J., Halecký, M., Ecorchard, P., Machálková, A., Medeiros, G.S., Hodan, J., Pavlova, E., Beneš, H., 2021. Sustainable microwave synthesis of biodegradable active packaging films based on polycaprolactone and layered ZnO nanoparticles. Polym. Degrad. Stabil. 190, 109625 https://doi.org/10.1016/j.polymdegradstab.2021.109625.

Chaparro, F.J., Presley, K.F., Coutinho da Silva, Marco, A., Mandan, N., Colachis, M.L., Posner, M., Arnold, R.M., Fan, F., Moraes, C.R., Lannutti, J.J., 2019. Sintered electrospun poly (ε-caprolactone)–poly (ethylene terephthalate) for drug delivery. J. Appl. Polym. Sci. 136 (26), 47731 https://doi.org/10.1002/app.47731.

Chatani, Y., Okita, Y., Tadokoro, H., Yamashita, Y., 1970. Structural studies of polyesters. III. Crystal structure of poly-ε-caprolactone. Polym. J. 1 (5), 555–562. https://doi.org/10.1295/polymj.1.555.

Chen, H., Hsiao, M., 1998. Morphological structure induced by combined crystallization and liquid− liquid demixing in poly (ethylene terephthalate)/poly (ether imide) blends. Macromolecules 31 (19), 6579–6584. https://doi.org/10.1021/ma980700c.

da Rocha, Viana Maurat, Lizandra, Merat, L.C., de Menezes, L.R., Finotelli, P.V., da Silva, , Paulo Sergio Rangel Cruz, Tavares, M.I.B., 2019. Extract of Curcuminoids Loaded on Polycaprolactone and Pluronic Nanoparticles: Chemical and Structural Properties. Applied Nanoscience, pp. 1–16. https://doi.org/10.1007/s13204-019-01197-w.

De Falco, F., Avolio, R., Errico, M.E., Di Pace, E., Avella, M., Cocca, M., Gentile, G., 2021. Comparison of biodegradable polyesters degradation behaviour in sand. J. Hazard Mater., 126231 https://doi.org/10.1016/j.jhazmat.2021.126231.

Delgado, B., Carrêlo, H., Loureiro, M.V., Marques, A.C., Borges, J.P., Cidade, M.T., 2021. Injectable hydrogels with two different rates of drug release based on pluronic/water system filled with poly (ε-caprolactone) microcapsules. J. Mater. Sci. 56 (23), 13416–13428. https://doi.org/10.1007/s10853-021-06156-x.

Doppalapudi, S., Jain, A., Khan, W., Domb, A.J., 2014. Biodegradable polymers—an overview. Polym. Adv. Technol. 25 (5), 427–435. https://doi.org/10.1002/pat.3305.

Fakhrali, A., Nasari, M., Poursharifi, N., Semnani, D., Salehi, H., Ghane, M., Mohammadi, S., 2021. Biocompatible graphene-embedded PCL/PGS-based nanofibrous scaffolds: a potential application for cardiac tissue regeneration. J. Appl. Polym. Sci., 51177 https://doi.org/10.1002/app.51177.

Gupta, P.K., Gahtori, R., Govarthanan, K., Sharma, V., Pappuru, S., Pandit, S., Mathuriya, A.S., Dholpuria, S., Bishi, D.K., 2021. Recent trends in biodegradable polyester Nanomaterials for Cancer therapy. Mater. Sci. Eng. C, 112198. https://doi.org/10.1016/j.msec.2021.112198.

Hassanzadeh, S., Khoee, S., Farrokhi, V., Mahdavi, M., Foroumadi, A., 2014. Mixed micellar nanoparticles based on PCL-PEG-PPO-PEG-PCL pentablocks. J. Polym. Res. 21 (7), 1–12. https://doi.org/10.1007/s10965-014-0508-2.

Heeley, E.L., Hughes, D.J., El Aziz, Y., Taylor, P.G., Bassindale, A.R., 2014. Morphology and crystallization kinetics of polyethylene/long alkyl-chain substituted Polyhedral Oligomeric Silsesquioxanes (POSS) nanocomposite blends: a SAXS/WAXS study. Eur. Polym. J. 51, 45–56. https://doi.org/10.1016/j.eurpolymj.2013.11.020.

Jackson, J.K., Springate, C.M., Hunter, W.L., Burt, H.M., 2000. Neutrophil activation by plasma opsonized polymeric microspheres: inhibitory effect of Pluronic F127. Biomaterials 21 (14), 1483–1491. https://doi.org/10.1016/S0142-9612(00)00034-X.

Kalogeras, I.M., Brostow, W., 2009. Glass transition temperatures in binary polymer blends. J. Polym. Sci. B Polym. Phys. 47 (1), 80–95. https://doi.org/10.1002/polb.21616.

Ketelaars, A., Papantoniou, Y., Nakayama, K., 1997. Analysis of the density and the enthalpy of poly (ε-caprolactone)-polycarbonate blends: amorphous phase compatibility and the effect of secondary crystallization. J. Appl. Polym. Sci. 66 (5), 921–927. https://doi.org/10.1002/(SICI)1097-4628(19971031)66:53.0.CO;2-Q.

Kurusu, R.S., Demarquette, N.R., Gauthier, C., Chenal, J., 2014. Effect of ageing and annealing on the mechanical behaviour and biodegradability of a poly (3-hydroxybutyrate) and poly (ethylene-co-methyl-acrylate-co-glycidyl-methacrylate) blend. Polym. Int. 63 (6), 1085–1093. https://doi.org/10.1002/pi.4616.

Labet, M., Thielemans, W., 2009. Synthesis of polycaprolactone: a review. Chem. Soc. Rev. 38 (12), 3484–3504. https://doi.org/10.1039/B820162P.

Lee, J., Chae, S., Lee, H., Kim, G.H., 2020. A 3D printing strategy for fabricating in situ topographical scaffolds using pluronic F-127. Additive Manufacturing 32. https://doi.org/10.1016/j.addma.2019.101023.

Li, W., Hu, Y., Shi, L., Zhang, X., Xiong, L., Zhang, W., Ullah, I., 2018. Electrospinning of Polycaprolactone/Pluronic F127 dissolved in glacial acetic acid: fibrous scaffolds fabrication, characterization and in vitro evaluation. J. Biomater. Sci. Polym. Ed. 29 (10), 1155–1167. https://doi.org/10.1080/09205063.2018.1439431.

Li, Y., Yao, S., Shi, H., Zhang, Y., Han, C., Yu, Y., 2021. Enhancing the crystallization of biodegradable poly (ε-caprolactone) using a polyvinyl alcohol fiber favoring nucleation. Thermochim. Acta 706, 179065.

Liu, N., Pan, J., Miao, Y., Liu, T., Xu, F., Sun, H., 2014. Electrospinning of poly (ε-caprolactone-co-lactide)/Pluronic blended scaffolds for skin tissue engineering. J. Mater. Sci. 49 (20), 7253–7262. https://doi.org/10.1007/s10853-014-8432-8.

Lu, B., Wang, G., Huang, D., Ren, Z., Wang, X., Wang, P., Zhen, Z., Zhang, W., Ji, J., 2018. Comparison of PCL degradation in different aquatic environments: effects of bacteria and inorganic salts. Polym. Degrad. Stabil. 150, 133–139. https://doi.org/10.1016/j.polymdegradstab.2018.02.002.

Ma, G., Song, C., 2007. PCL/poloxamer 188 blend microsphere for paclitaxel delivery: influence of poloxamer 188 on morphology and drug release. J. Appl. Polym. Sci. 104 (3), 1895–1899. https://doi.org/10.1002/app.25866.

Mei, L., Zhang, Y., Zheng, Y., Tian, G., Song, C., Yang, D., Chen, H., Sun, H., Tian, Y., Liu, K., 2009. A novel docetaxel-loaded poly (ε-caprolactone)/pluronic F68 nanoparticle overcoming multidrug resistance for breast cancer treatment. Nanoscale Res. Lett. 4 (12), 1530–1539. https://doi.org/10.1007/s11671-009-9431-6.

Mirhosseini, M.M., Haddadi-Asl, V., Zargarian, S.S., 2016. Fabrication and characterization of hydrophilic poly (ε-caprolactone)/pluronic P123 electrospun fibers. J. Appl. Polym. Sci. 133 (17) https://doi.org/10.1002/app.43345.

Pantani, R., Sorrentino, A., 2013. Influence of crystallinity on the biodegradation rate of injection-moulded poly (lactic acid) samples in controlled composting conditions. Polym. Degrad. Stabil. 98 (5), 1089–1096. https://doi.org/10.1016/j.polymdegradstab.2013.01.005.

Patricio, T., Bártolo, P., 2013. Thermal stability of PCL/PLA blends produced by physical blending process. Procedia Eng. 59, 292–297. https://doi.org/10.1016/j.proeng.2013.05.124.

Pitt, C.G., Chasalow, F.I., Hibionada, Y.M., Klimas, D.M., Schindler, A., 1981. Aliphatic polyesters. I. The degradation of poly (ε-caprolactone) in vivo. J. Appl. Polym. Sci. 26 (11), 3779–3787. https://doi.org/10.1002/app.1981.070261124.

Pohlmann, A.R., Fonseca, F.N., Paese, K., Detoni, C.B., Coradini, K., Beck, R.C., Guterres, S.S., 2013. Poly (ε-caprolactone) microcapsules and nanocapsules in drug delivery. Expet Opin. Drug Deliv. 10 (5), 623–638. https://doi.org/10.1517/17425247.2013.769956.

Rychter, M., Milanowski, B., Grześkowiak, B.F., Jarek, M., Kempiński, M., Coy, E.L., Borysiak, S., Baranowska-Korczyc, A., Lulek, J., 2019. Cilostazol-loaded electrospun three-dimensional systems for potential cardiovascular application: effect of fibers hydrophilization on drug release, and cytocompatibility. J. Colloid Interface Sci. 536, 310–327. https://doi.org/10.1016/j.jcis.2018.10.026.

Selli, F., Erdoğan, U.H., Hufenus, R., Perret, E., 2020. Mesophase in melt-spun poly (ε-caprolactone) filaments: structure–mechanical property relationship. Polymer 206, 122870. https://doi.org/10.1016/j.polymer.2020.122870.

Shaker, M.A., Elbadawy, H.M., Shaker, M.A., 2020. Improved solubility, dissolution, and oral bioavailability for atorvastatin-Pluronic® solid dispersions. Int. J. Pharm. 574, 118891.

Shalaev, E., Wu, K., Shamblin, S., Krzyzaniak, J.F., Descamps, M., 2016. Crystalline mesophases: structure, mobility, and pharmaceutical properties. Adv. Drug Deliv. Rev. 100, 194–211. https://doi.org/10.1016/j.addr.2016.04.002.

Stoclet, G., Seguela, R., Lefebvre, J., Rochas, C., 2010. New insights on the strain-induced mesophase of poly (d, l-lactide): in situ WAXS and DSC study of the thermo-mechanical stability. Macromolecules 43 (17), 7228–7237. https://doi.org/10.1021/ma101430c.

Strobl, G.R., Schneider, M., 1980. Direct evaluation of the electron density correlation function of partially crystalline polymers. J. Polym. Sci. Polym. Phys. Ed 18 (6), 1343–1359. https://doi.org/10.1002/pol.1980.180180614.

Vergara-Porras, B., Gracida-Rodríguez, J.N., Pérez-Guevara, F., 2016. Thermal processing influence on mechanical, thermal, and biodegradation behavior in poly (β-hydroxybutyrate)/poly (ε-caprolactone) blends: a descriptive model. J. Appl. Polym. Sci. 133 (27) https://doi.org/10.1002/app.43569.

Wang, H., Ji, J., Zhang, W., Zhang, Y., Jiang, J., Wu, Z., Pu, S., Chu, P.K., 2009. Biocompatibility and bioactivity of plasma-treated biodegradable poly (butylene succinate). Acta Biomater. 5 (1), 279–287. https://doi.org/10.1016/j.actbio.2008.07.017.

Werle, M., 2008. Natural and synthetic polymers as inhibitors of drug efflux pumps. Pharm. Res. (N. Y.) 25 (3), 500–511. https://doi.org/10.1007/s11095-007-9347-8.

Wu, B., Takeshita, N., Wu, Y., Vijayavenkataraman, S., Ho, K.Y., Lu, W.F., Fuh, J.Y.H., 2018. Pluronic F127 blended polycaprolactone scaffolds via e-jetting for esophageal tissue engineering. J. Mater. Sci. Mater. Med. 29 (9), 140. https://doi.org/10.1007/s10856-018-6148-z.

Wunderlich, B., 1999. A classification of molecules, phases, and transitions as recognized by thermal analysis. Thermochim. Acta 340, 37–52. https://doi.org/10.1016/S0040-6031(99)00252-X.

Yang, X., Yin, Z., Zhang, X., Zhu, Y., Zhang, S., 2020. Fabrication of emulsion-templated macroporous poly (ε-caprolactone) towards highly effective and sustainable oil/water separation. Polymer 204, 122852. https://doi.org/10.1016/j.polymer.2020.122852.

Zaman, H.U., Beg, M., 2015. Improvement of physico-mechanical, thermomechanical, thermal and degradation properties of PCL/gelatin biocomposites: effect of gamma radiation. Radiat. Phys. Chem. 109, 73–82. https://doi.org/10.1016/j.radphyschem.2014.12.011.

Zargarian, S.S., Haddadi-Asl, V., Kafrashian, Z., Azarnia, M., Mirhosseini, M.M., Seyedjafari, E., 2019. Surfactant-assisted-water-exposed versus surfactant-aqueous-solution-exposed electrospinning of novel super hydrophilic polycaprolactone based fibers: analysis of drug release behavior. J. Biomed. Mater. Res. 107 (3), 597–609. https://doi.org/10.1002/jbm.a.36575.

Zhou, Y., Wang, P., Ruan, G., Xu, P., Ding, Y., 2021. Synergistic effect of P [MPEGMA-IL] modified graphene on morphology and dielectric properties of PLA/PCL blends. ES Mater. Manuf. 11, 20–29.

Zhu, B., He, Y., Yoshie, N., Asakawa, N., Inoue, Y., 2004. Partial phase segregation in strongly hydrogen-bonded and miscible blends. Macromolecules 37 (9), 3257–3266. https://doi.org/10.1021/ma035889t.